NANO LETTERS
Letter
pubs.acs.org/NanoLett

Dynamic Evolution of Conducting Nanofilament in Resistive Switching Memories

Jui-Yuan Chen,[†] Cheng-Lun Hsin,[†,‡,§] Chun-Wei Huang,[†] Chung-Hua Chiu,[†] Yu-Ting Huang,[†] Su-Jien Lin,[‡] Wen-Wei Wu,[*,†] and Lih-Juann Chen[‡]

[†]Department of Materials Science and Engineering, National Chiao Tung University, Hsinchu City, Taiwan 300
[‡]Department of Materials Science and Engineering, National Tsing Hua University, Hsinchu City, Taiwan 300
[§]Department of Electrical Engineering, National Central University, Zhongli City, Taiwan 320

Supporting Information

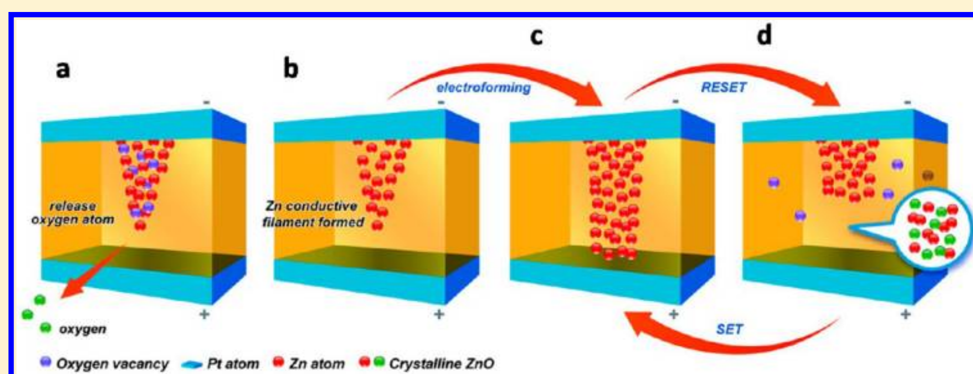

ABSTRACT: Resistive random access memory (ReRAM) has been considered the most promising next-generation nonvolatile memory. In recent years, the switching behavior has been widely reported, and understanding the switching mechanism can improve the stability and scalability of devices. We designed an innovative sample structure for in situ transmission electron microscopy (TEM) to observe the formation of conductive filaments in the Pt/ZnO/Pt structure in real time. The corresponding current−voltage measurements help us to understand the switching mechanism of ZnO film. In addition, high-resolution transmission electron microscopy (HRTEM) and electron energy loss spectroscopy (EELS) have been used to identify the atomic structure and components of the filament/disrupted region, determining that the conducting paths are caused by the conglomeration of zinc atoms. The behavior of resistive switching is due to the migration of oxygen ions, leading to transformation between Zn-dominated ZnO_{1-x} and ZnO.

KEYWORDS: *In situ TEM, RRAM, resistive switching, nanofilament, redox, unipolar*

Traditional charge-based memory, such as floating-gate nonvolatile semiconductor memory (FG-NVSM), will face severe problems when the scaling limit is approached. In this circumstance, the developing nonvolatile memory (NVM) has attracted extensive attention due to high performance in retention, high density, low cost, fast write/read speed, and low power consumption.[1] However, the noncharge-based memory technologies have encountered difficulties in retaining electrons at shrinking sizes. Lee et al. clearly indicates two important factors that must be realized for the miniaturization of memory to the nanometer scale.[2] The switching current must be scaled down, and the memory must scale down beyond the 30 nm node technology. Therefore, a revolutionary nonvolatile memory, resistance switching random access memory (ReRAM), has been considered to be the candidate to overcome the physical and technological limitations and fulfill the essential requirements for 3-D integrated circuit architecture in the next generation.[2−8]

Generally, a ReRAM device has a metal−insulator−metal (MIM) or metal−semiconductor−metal (MSM) structure. A variety of materials in the insulator configuration, such as TaO_2,[2] NiO,[9] CuO,[10] TiO_2,[11,12] $SrTiO_3$,[13,14] and ZnO[15−18] have been recently explored to show resistive switching behavior. Although many of the materials were shown to have resistive switching properties, the switching mechanism still remains mysterious. In previous reports, the switching mechanism can be attributed to the cation migration, that is, the metal diffusion from the electrodes into the insulator resulting in conductive bridge,[19−22] or anion migration, that is, transition metal oxides forming conductive filament by local redox processes.[11,23] However, the ex situ observations could only investigate the initial and final state and critical

Received: April 30, 2013
Revised: June 21, 2013
Published: July 15, 2013

 © 2013 American Chemical Society

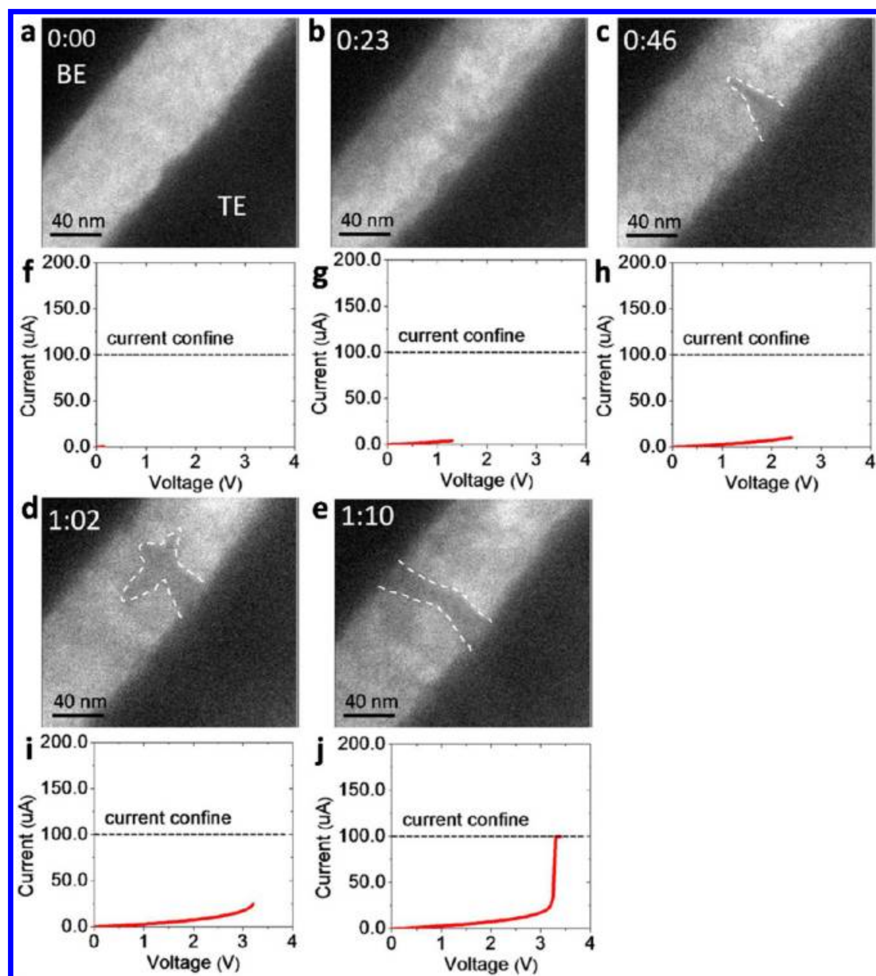

Figure 1. A series of in situ TEM images clipped from the video and the corresponding *I*−*V* measurements. (a) At the start of recording, the ZnO was in the initial state. (b) When voltage was applied, the contrast of ZnO enhanced near both of the electrodes. (c) A conical-shaped filament generated near the top electrode. The white dashed line highlights the filament. (d) The filament transformed into a dendritic shape, but the filament was still not connected to the bottom electrode. The specimen was still in the high-resistance state. (e) The columnar filament passed through the ZnO film connecting the top and bottom electrodes. The corresponding *I*−*V* curve (f to j) shows the switching characteristic with filament formation, which revealed that the switching behavior is due to the filaments.

information during resistive switching process is lost. Additionally, the thermodynamics and electrochemical reactions of the resistive switching mechanisms are still not fully understood. For this purpose, the in situ observation of filament formation is essential for the study of the switching process.

There have been numerous research reports on the thermodynamics and electrochemistry of nanomaterials by in situ transmission electron microscopy (TEM).[16,24−28] Here, we designed a test structure for in situ TEM observation to see the growth of conductive filaments in real time (Figure S1a−f of the Supporting Information). ZnO was selected as a potential ReRAM material since it has been demonstrated to be a wide bandgap semiconductor with unipolar resistance switching behavior (positive or negative bias can be used for set and reset), scalability, and a low reset current.[15] The in situ TEM measurements at various voltages are essential since not only the low/high resistance states but also the intermediate states should be located at the same position of the device. These direct observations provide us the answer to the enigmatic question: how do the filaments develop as the voltage applied? We successfully demonstrate that the resistive switching of a Pt/ZnO/Pt structure is associated with the formation and rupture of conductive filaments, which is clearly validated by the in situ TEM observations. Furthermore, the detailed high-resolution (HR)TEM and electron energy loss spectroscopy (EELS) has been used to identify the structure of the filaments in ZnO, which enables us to determine that the dominant conducting species is zinc. We demonstrate that the behavior of resistive switching is due to the migration of oxygen ions, leading to a conversion between Zn-dominated ZnO_{1-x} and ZnO. The simultaneous electrical switching confirmed that the resistance switching was induced by the redox between zinc oxide and zinc metallic conductive filaments. An electrochemical redox reaction model is proposed to explain the resistive switching phenomenon.

The sample was prepared by RF magnetron sputtering deposition of a 100-nm-thick ZnO thin film which was sandwiched between the Pt top and bottom electrodes. For the purpose of real time observation, the sample was cut into a 100 nm high × 1 μm wide × 50 nm thick piece by a focused ion beam (FIB). The details of the sample preparation are included in the Supporting Information. The switching behavior of this sample was measured by applying a negative bias to the top electrode with the bottom grounded. To investigate the conjectured composition of a conductive filament, we focus on the filament forming process since the most dramatic

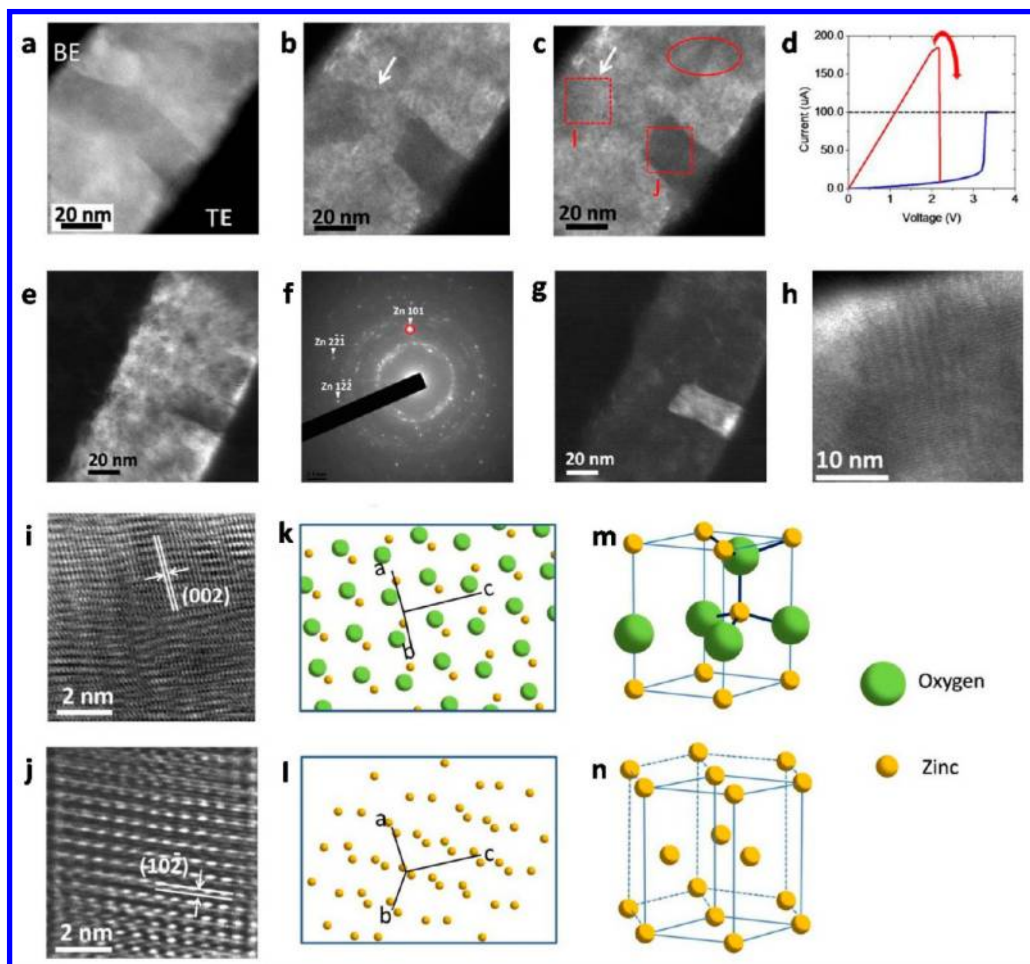

Figure 2. In situ TEM images of the reset process using the unipolar resistive switching method. (a) The start of recording; (b) intermediate state; (c) final state of the ruptured filament after the reset process. (d) The corresponding $I-V$ curve in red; the blue line corresponds to the forming process as a comparison. (e) The other conductive filament in the same in situ specimen, indicating that the switching behavior is caused by multifilament formation and rupture. (f) The selected area diffraction pattern of the conductive filament in Figure 2e. The Zn (101) diffraction spot is marked with the red circle. (g) The corresponding dark-field image obtained from the diffraction spot marked as a circle in the diffraction pattern f. (h) The Moire fringes can be observed at the disrupted region from a high-magnification TEM image. (i) The HRTEM image along the ⟨110⟩ zone axis in the disrupted region, revealing that the conductive filaments were converted back to ZnO_{1-x}. (j) The HRTEM of the "zinc "conductive filament along the ⟨231⟩ zone axis has been identified. (k) Solid-sphere model of ZnO in a wurtzite structure along the ⟨110⟩ zone axis. The coordinate lines are the unit cell vectors. (l) Solid-sphere model of zinc in a HCP structure along the ⟨231⟩ zone axis. The 3-D schematic illustrations of (m) a ZnO unit cell and (n) a zinc unit cell, respectively, showing that the zinc atoms position remain the same as the oxygen ions diffuse out.

change in structure would be expected at this step. The in situ observation and the corresponding $I-V$ measurements are shown in Figure 1. The ZnO film is in the initial high resistance state (Figure 1a and f) and is electroformed by using a voltage sweep process (sweep rate 0.05 V/s) with a compliance current of 10^{-4} ampere. When the voltage was gradually raised to 1.3 V, the contrast of the ZnO film enhanced at the region near the electrodes (Figure 1b and g), which was possibly attributing to electronic charge injection and/or ionic charge displacement effects. In many transition metal oxides, oxygen ion defects and oxygen vacancies are much more mobile than cations under an external electric field.[3] The oxygen ions that migrated due to the electric field in the oxide semiconductor layer could cause the oxygen-vacancy doping, resulting in the slight decrease of the resistance.[12,29] The oxygen vacancies could be created when the oxygen ions (O^{2-}) are retracted from the matrix by the external field and thermal effects. The formation of one oxygen vacancy can be described as follows:

$$O_O^{\times} \rightarrow V_O^{\bullet\bullet} + O_i^{''} \quad (1)$$

The equation is based on Kroger–Vink notation; the small marks at the upper right corner and lower right corner denote electric charges and positions, respectively.

The electrochemical reaction leads to the incorporation of oxygen ions (O^{2-}) toward the Pt anode electrode (as shown in Figure S2). When a higher voltage is applied to the sample, the oxygen vacancies will gather at the cathode (top electrode, TE) due to the repulsion of oxygen ions (O^{2-}). Once a sufficient concentration of oxygen vacancies gathers near the electrode and the charges are balanced by electrons from the applied bias, the oxygen vacancies rearrange to form an ordered structure, resulting in conductive filaments of crystalline zinc near the top electrode (the darker contrast highlighted by the white dashed line in Figure 1c). The proposed reduction reaction is:

$$Zn_{Zn}^{\times} + V_o^{\bullet\bullet} + 2e^- \rightarrow Zn_{Zn}^{\times} \quad (2)$$

$$O_i^{''} \rightarrow 1/2O_2 + 2e^- \quad (3)$$

dx.doi.org/10.1021/nl4015638 | Nano Lett. 2013, 13, 3671–3677

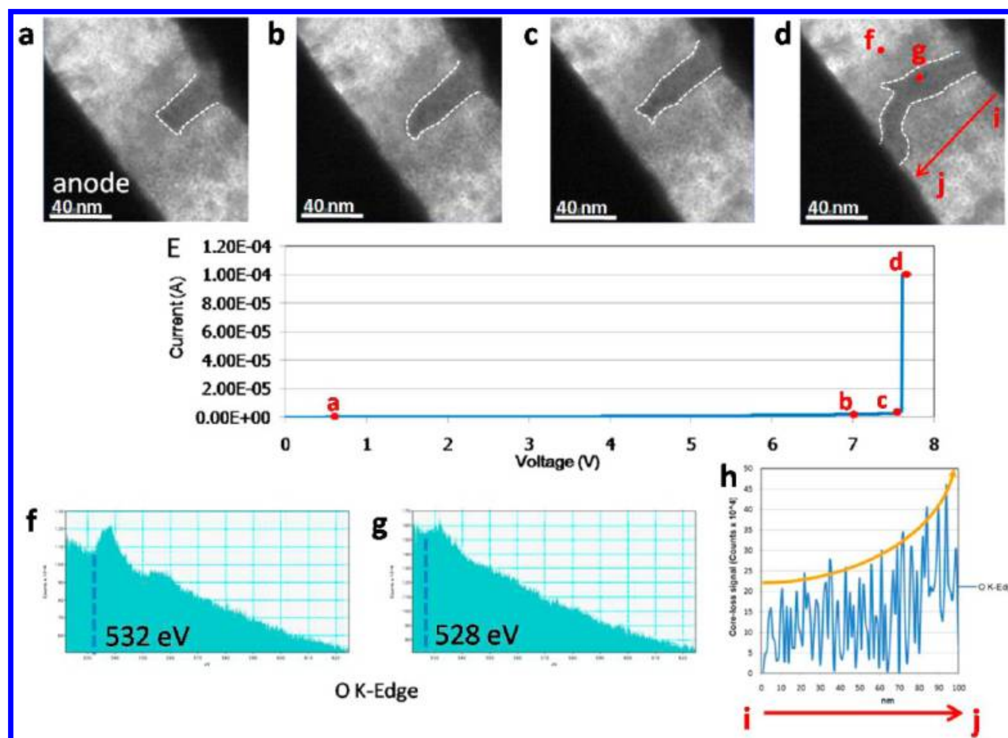

Figure 3. | A series of in situ set process of TEM image clipped from the video and the corresponding *I*−*V* measurement. This in situ set data is acquired from another sample. The labels of the TEM image (a−d) correspond to the red dot marked in the *I*−*V* curve (e). From the TEM images, the sec process resumed from the residual filament. As the dramatic switching of resistive state occurred, the conductive filament penetrated through the ZnO film and connected the top and bottom electrodes. (f−g) The TEM—EELS spectra correspond to the red dots marked in the TEM image d. Comparing the difference between the matrix f and filament g: (1) the unbounded oxygen ions located in the matrix, and (2) the neighboring ZnO matrix served as the oxygen reservoir. (h) The EELS line scan from i to j in the matrix region in d. The oxygen tends to gather toward the anode as applying bias.

The formation of a metallic conductive filament would lead to an enhancement of the electric field, resulting in the continuous growth of filament in the same region. The morphology of the conductive filaments transformed as the applied voltage increased (Figure 1c and d), that is, from a conical shape to a dendritic shape, and could be explained by electric field simulation.[3,30] In the simulation model, there would be a larger charge density between the region with a smaller radius of curvature and shortened distance with electrodes, contributing to the stronger electric field strength at the filament tip. Therefore, the electric field would drive the oxygen ions to move and change the filament shape from a cone to dendrite geometry. Meanwhile, the switching behavior is correlated to the formation of connected filaments. The dramatic switching of resistive state occurred at 3.25 V (Figure 1j) when a cylindrical conductive filament penetrated through the ZnO film and connected the top and bottom electrodes. When the conductive filament connected the top and bottom electrodes, the electrical field on the ZnO matrix would drop. The oxygen ion-vacancy pair (eq 1) caused by electric field would be restrained. The higher concentration of oxygen ions near the anode would quickly fill back to vacancies, thereby dematerializing the filament branch through equilibrium. The resistances for the in situ sample are $2.56 \times 10^5\ \Omega$ for the initial state and $1.12 \times 10^4\ \Omega$ for LRS.

The rewriting process and its ex situ image are shown in Figure S3, indicating that this specimen can operate repetitively with ReRAM properties.

To further confirm the conductive filament switching mechanism, a reset operation was also performed in TEM in the same region in Figure 1, as shown in Figure 2a−c. In our work, the unipolar resistive switching measurement was used since the system is a symmetrical MSM structure and independent with ionic transport from the electrode metal. The switching OFF was the result of the rupture of the conductive filaments by Joule heating, which has been proposed in models of unipolar switching.[3,31]

When the voltage was raised to 2.2 V without setting compliance current, the current suddenly drops as a typical of unipolar switching (Figure 2d). This thermochemical reaction was observed in the top right corner of the Figure 2c (marked with the red circle). The contrast of the image is enhanced because the oxygen ions were supplied to the conductive filament from the neighboring ZnO. Since the experiment was operating in a high vacuum environment, the supply of oxygen ions could only come from the oxygen migration from the neighboring oxide matrix. The EDX mapping (Figure S2) of the O and the EELS line scan (Figure 3h) support our explanation to the role of electric field and ZnO matrix. The reaction could be given by:

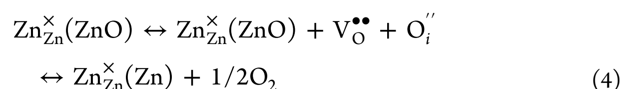

$$\mathrm{Zn}_{\mathrm{Zn}}^{\times}(\mathrm{ZnO}) \leftrightarrow \mathrm{Zn}_{\mathrm{Zn}}^{\times}(\mathrm{ZnO}) + \mathrm{V}_{\mathrm{O}}^{\bullet\bullet} + \mathrm{O}_i'' \leftrightarrow \mathrm{Zn}_{\mathrm{Zn}}^{\times}(\mathrm{Zn}) + 1/2\mathrm{O}_2 \quad (4)$$

The rupture of the conductive filaments occurred from the middle to bottom electrode, and partial filaments remained near the top electrode (Figure 2b and c). It is the result of oxygen ion migration easily toward the anode[32,33] (Figure S2) or the sample structure at the initial electroforming process which could lead to a hot spot generated in the middle of the

dx.doi.org/10.1021/nl4015638 | *Nano Lett.* 2013, 13, 3671−3677

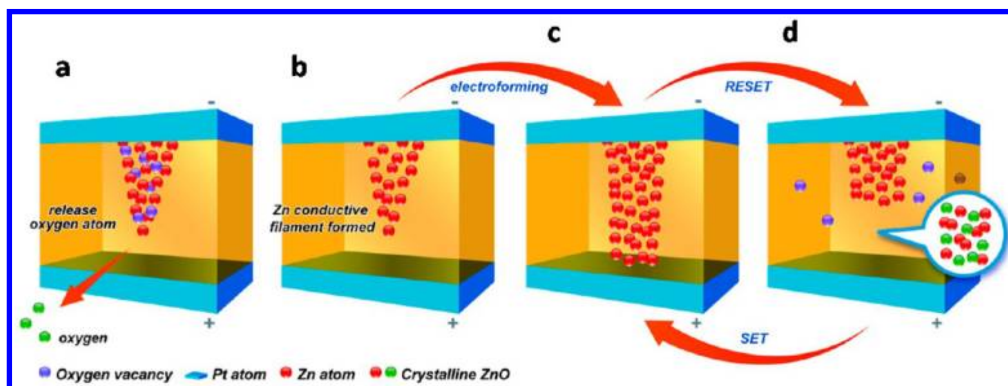

Figure 4. Schematic diagram for the mechanism of resistive switching in Pt/ZnO/Pt devices. (a) The release of oxygen gas (O_2) leads to the oxygen vacancies in the bulk of ZnO. (b) The migration of the mobile oxygen vacancies toward the cathode (oxygen ions (O^{2-}) toward the anode) and the rearrangement of Zn-dominated ZnO_{1-x}. (c) The precipitation of Zn atoms to form a conductive filament. (d) The rupture of the filament. When the energy of Joule heating provides to the thermochemical reaction, the filament will rupture and change back to ZnO. Owing to the migration of oxygen ions, the ReRAM resets back to the off state.

filament when Joule heating increases.[14] The Joule heating generated by the applied electric field provided energy to the thermochemical reaction. One may argue that the local temperature heating of the specimen by the electron beam might cause the thermochemical reaction. In fact, we also found the other conductive filaments elsewhere in the specimen, indicating that the rupture of conductive filaments can still be achieved without electron beam exposure, as shown in Figure 2e. The bright field image is the other conductive filament. We found that both of the conductive filaments ruptured during the reset operation, which means the switching behaviors were caused by multifilament formation and rupture in the thin film ReRAM device.[3,9,21,28] The diffraction pattern of the as-prepared sample (Figure S4) shows that the ZnO film deposited by RF sputtering was polycrystalline. Moreover, after the electrical operations, some extra diffraction spots, which can be attributed to the conductive zinc filaments, appear. This filament with low index of planes benefits the dark field imaging. (The rest of the diffraction rings in Figure 2 are undoubtedly from polycrystalline ZnO; more detailed discussions are in Figure S4.) The dark-field image (Figure 2g) obtained from the diffraction spot marked with a red-line circle in Figure 2f demonstrated that the disrupted region changed back to ZnO. Furthermore, the distinct shape of the filaments in dark field imaging (Figure 2g) matched with the bright field observations (Figure 2e). This is a strong evidence that the filament was indeed a newly generated phase (Zn-dominated ZnO_{1-x}), not just an oxygen-deficient phase. (The resistance-temperature characteristic is shown in Figure S5, indicating that the conducting nanofilament is a metallic phase.)

Owning to the conductive filament embedded in the ZnO matrix, the structure analysis is a good method to identify its composition. Figure 2h–n show detailed information of the filament after the reset process. The conductive filament along the ⟨231⟩ zone axis has been identified as zinc from the HRTEM image, as shown in Figure 2j. As a comparison, the HRTEM image in the disrupted region revealed that the conductive filaments converted back to ZnO along the ⟨110⟩ zone axis, as shown in Figure 2i. The structural model for the process of set/reset was represented in Figure 2k–n. ZnO has a wurtzite structure with $a = b = 3.249$ nm, $c = 5.205$ nm, $\alpha = \beta = 90°$, and $\gamma = 120°$, as shown in Figure 2m, while Zn has a HCP structure where $a = b = 2.665$ nm, $c = 4.946$ nm, $\alpha = \beta = 90°$, and $\gamma = 120°$, as shown in Figure 2n. The 3-D schematic illustrations matched with the atomic image along the zone axis: the ZnO in a wurtzite structure along the ⟨110⟩ zone axis (Figure 2k), and the Zn in a HCP structure along the ⟨231⟩ zone axis (Figure 2l).

As mentioned before, the mobility of oxygen ion defects and oxygen vacancies is much more enhanced under external electric field, as shown in the EDX mapping (Figure S2) and the EELS line scan (Figure 3h). With the atomic image and the schematic illustrations, we found that the oxygen migration dominated the formation of conductive filaments. From the HRTEM analysis (Figure 2i–j), the crystalline of the filament can also be observed. Oxygen vacancy rearrangement is because the crystalline metal phase would benefit the electron transmission as the electric field provides energy for rearrangement. Although, we did not directly observe the oxygen vacancy rearrangement, it can be confirmed through comparing with the in situ experiment (Figure 1), where the dark contrast in Figure 1 was attributed to oxygen vacancy rearrangement. To reveal the details of the relationship between the conductive filament and the disrupted region, the angles between $\langle 2\bar{2}3\rangle$ direction of zinc atoms in Zn and ZnO (the zinc atom is displaced from the cell corner along the $\langle 2\bar{2}3\rangle$ direction) and their (001) plane has been calculated to be 31.88° for Zn and 35.78° for ZnO theoretically.

Also, the actual value of the (001) plane can be measured from the HRTEM images. The angle difference between ZnO and Zn (001) plane rotated about 3.3°. This result shows that the actual value is consistent with the theoretical value, proving that the zinc atoms do not disappear from specimens. The Zn atoms would be slightly distorted as the structure changed from ZnO to Zn due to the rotation of atomic position (c-axis rotated 3.3°) and different atomic spacing (difference between c-axis is 0.259 nm). Therefore, we found that the switching mechanism is indeed triggered by oxygen ions and vacancies migration. The disrupted region shows regular orientation, as shown in Figure 2i. The moire fringes can be observed in the HRTEM image in the disrupted region (ZnO) after the reset process (Figure 2h). This is due to the slight rotation by an angle of 3.3 degrees when the oxygen atoms backfill to zinc.

The original device was damaged due to testing (including EDX analysis) for other purposes. The in situ sec data is acquired from another sample (Figures 3a–d). We also performed the test of forming, set, and reset repeatedly, and the result shows good reproducibility. This result provides

more evidence of this resistive switching behavior in the ZnO. Then the on/off voltage would be surely a bit different because of geometrical differences between devices. The higher set voltage could also be attributed to higher series resistance of the Si substrate (please refer to Supporting Information: Material and Methods). The set process resumed from the residual filament. As the dramatic switching of resistive state occurred (Figure 3e), the conductive filament penetrated through the ZnO matrix and connected the top and bottom electrodes. The rupture and reconnection of filament occurred near the anode may result from the reserved oxygen in the insulator closing to anode, as shown in Figure S2 and Figure 3h. The rewriting process of the *I*−*V* measurements and its in situ TEM are provided and demonstrated the complete resistive-switching properties in ZnO.

The switching behavior is induced by the redox reaction; therefore, the reservoir of the oxygen would be an important issue for stability and reliability. Here shows the differences of the oxygen K-edge signal between filament (Figure 3g) and ZnO matrix (Figure 3f). First, the signal of oxygen decreased obviously in filament region (Figure 3f), which confirmed the out-diffusion of oxygen from the filament. The oxygen signal detected in the filament region would result from the surrounding ZnO matrix of the embed Zn-dominated ZnO_{1-x} filament. Second, the threshold energy of oxygen K-edge shifted from 532 eV to lower energy (528 eV) in filament region, demonstrating the less unbounded oxygen ions and structural defects in filament.[18] This EELS information demonstrated that the behavior of resistive switching is due to the migration of oxygen ions, leading to transformation between Zn-dominated ZnO_{1-x} and ZnO. (The TEM-EDX data are also included in the Supporting Information, Figure S6.)

Figure 4 illustrates a schematic for the switching mechanism: the oxygen vacancies are created as the oxygen ions (O^{2-}) are moving toward the Pt anode electrode. When large concentrations of oxygen vacancies gather at the cathode, the zinc atoms rearrange their position/structure from oxygen vacancy doped ZnO to crystalline Zn-dominated ZnO_{1-x}. During the reset process, the migration of the neighboring oxygen ions disrupted the conductive filaments near the anode. Since the electroforming process rearranged the zinc atoms into a crystalline phase, the structure of the disrupted region should also be periodic.

In summary, we have successfully observed the resistive switching behavior and structural change via in situ TEM and demonstrated that the switching behavior is related to the formation and rupture of conductive filaments. The study enriches our understanding of material behaviors in memristive memory devices. HRTEM has been used to identify the structure of conductive filaments and showed that the filament is composed of metallic zinc. In the Pt/ZnO/Pt systems, the structure of the conductive filaments, the impact of thermal effects, the connection of the electrode and filament formation/disruption, and the morphology of the metallic conductive filaments on the nanometer scale has been clarified. Also, the reservation and distribution of oxygen for simple MIM structure have been clearly identified. These points are essential but have eluded in previous study. The switching experiments confirmed that the set/reset behavior is induced by the migration of oxygen ions, leading to the conversion between Zn-dominated ZnO_{1-x} and ZnO. An electrochemical redox reaction model was also proposed and explained the resistive switching phenomenon.

■ ASSOCIATED CONTENT

Supporting Information

Materials and methods, composition analysis and electrical properties of nanofilaments, and the *I*−*V* switching characteristics (pdf), plus a video (avi) of the in situ TEM measurements. This material is available free of charge via the Internet at http://pubs.acs.org.

■ AUTHOR INFORMATION

Corresponding Author

*E-mail: WWWu@mail.nctu.edu.tw.

Author Contributions

J.Y.C. fabricated the sample and performed electrical switching experiments. J.Y.C. and C.W.H. performed the FIB and TEM experiments. J.Y.C., C.W.H., Y.T.H., and C.H.C. performed the in situ switching experiments. J.Y.C. and W.W.W. analyzed the diffraction data and atomic structure. J.Y.C., C.L.H., and W.W.W. conceived the study and designed the research. J.Y.C. performed the experiments with the support from S.J.L. and L.J.C. J.Y.C., C.L.H., W.W.W., and L.J.C. wrote the paper.

Notes

The authors declare no competing financial interest.

■ ACKNOWLEDGMENTS

The authors W.W.W. and L.J.C. acknowledge the support from NSC Grants 100-2628-E-009-023-MY3, 100-2120-M-007-008, and 98-2221-E-007-104-MY3. We also thank Dr. W. C. Chien and Dr. M. S. Lee of Macronix company for giving us professional advices on device operation and mechanism discussion.

■ REFERENCES

(1) Burr, G. W.; Kurdi, B. N.; Scott, J. C.; Lam, C. H.; Gopalakrishnan, K.; Shenoy, R. S. *IBM J. Res. Dev.* **2008**, *52*, 449.

(2) Lee, M.-J.; Lee, C. B.; Lee, D.; Lee, S. R.; Chang, M.; Hur, J. H.; Kim, Y.-B.; Kim, C.-J.; Seo, D. H.; Seo, S.; Chung, U. I.; Yoo, I.-K.; Kim, K. *Nat. Mater.* **2011**, *10*, 625.

(3) Waser, R.; Aono, M. *Nat. Mater.* **2007**, *6*, 833.

(4) Jo, S. H.; Kim, K.-H.; Lu, W. *Nano Lett.* **2009**, *9*, 870.

(5) Kügeler, C.; Meier, M.; Rosezin, R.; Gilles, S.; Waser, R. *Solid-State Electron.* **2009**, *53*, 1287.

(6) Wei, L.; Jeong, D. S.; Kozicki, M.; Waser, R. *MRS Bull.* **2012**, *37*, 124.

(7) Yang, J. J.; Inoue, I. H.; Mikolajick, T.; Hwang, C. S. *MRS Bull.* **2012**, *37*, 131.

(8) International Technology Roadmap for Semiconductor 2011, www.itrs.net/Links/2011ITRS/Home2011.htm.

(9) Seo, S.; Lee, M. J.; Seo, D. H.; Jeoung, E. J.; Suh, D. S.; Joung, Y. S.; Yoo, I. K.; Hwang, I. R.; Kim, S. H.; Byun, I. S.; Kim, J. S.; Choi, J. S.; Park, B. H. *Appl. Phys. Lett.* **2004**, *85*, 5655.

(10) Dong, R.; Lee, D. S.; Xiang, W. F.; Oh, S. J.; Seong, D. J.; Heo, S. H.; Choi, H. J.; Kwon, M. J.; Seo, S. N.; Pyun, M. B.; Hasan, M.; Hwang, H. *Appl. Phys. Lett.* **2007**, *90*, 042107−3.

(11) Kwon, D.-H.; Kim, K. M.; Jang, J. H.; Jeon, J. M.; Lee, M. H.; Kim, G. H.; Li, X.-S.; Park, G.-S.; Lee, B.; Han, S.; Kim, M.; Hwang, C. S. *Nat. Nanotechnol.* **2010**, *5*, 148.

(12) Yang, J. J.; Pickett, M. D.; Li, X.; Ohlberg-Douglas, A. A.; Stewart, D. R.; Williams, R. S. *Nat. Nanotechnol.* **2008**, *3*, 429.

(13) Szot, K.; Speier, W.; Bihlmayer, G.; Waser, R. *Nat. Mater.* **2006**, *5*, 312.

(14) Janousch, M.; Meijer, G. I.; Staub, U.; Delley, B.; Karg, S. F.; Andreasson, B. P. *Adv. Mater.* **2007**, *19*, 2232.

(15) Chang, W.-Y.; Lai, Y.-C.; Wu, T.-B.; Wang, S.-F.; Chen, F.; Tsai, M.-J. *Appl. Phys. Lett.* **2008**, *92*, 022110−3.

(16) Huang, Y.-T.; Yu, S.-Y.; Hsin, C.-L.; Huang, C.-W.; Kang, C.-F.; Chu, F.-H.; Chen, J.-Y.; Hu, J.-C.; Chen, L.-T.; He, J.-H.; Wu, W.-W. *Anal. Chem.* **2013**, *85*, 3955.
(17) Song, J.; Zhang, Y.; Xu, C.; Wu, W.; Wang, Z. L. *Nano Lett.* **2011**, *11*, 2829.
(18) Huang, C.-H.; Huang, J.-S.; Lin, S.-M.; Chang, W.-Y.; He, J.-H.; Chueh, Y.-L. *ACS Nano* **2012**, *6*, 8407.
(19) Yang, Y. C.; Pan, F.; Liu, Q.; Liu, M.; Zeng, F. *Nano Lett.* **2009**, *9*, 1636.
(20) Choi, S.-J.; Park, G.-S.; Kim, K.-H.; Cho, S.; Yang, W.-Y.; Li, X.-S.; Moon, J.-H.; Lee, K.-J.; Kim, K. *Adv. Mater.* **2011**, *23*, 3272.
(21) Cho, B.; Yun, J.-M.; Song, S.; Ji, Y.; Kim, D.-Y.; Lee, T. *Adv. Funct. Mater.* **2011**, *21*, 3976.
(22) Yang, Y.; Gao, P.; Gaba, S.; Chang, T.; Pan, X.; Lu, W. *Nat. Commun.* **2012**, *3*, 732.
(23) Yao, J.; Sun, Z.; Zhong, L.; Natelson, D.; Tour, J. M. *Nano Lett.* **2010**, *10*, 4105.
(24) Chen, K.-C.; Wu, W.-W.; Liao, C.-N.; Chen, L.-J.; Tu, K. N. *Science* **2008**, *321*, 1066.
(25) Kim, B. J.; Tersoff, J.; Kodambaka, S.; Reuter, M. C.; Stach, E. A.; Ross, F. M. *Science* **2008**, *322*, 1070.
(26) Lin, Y.-C.; Lu, K.-C.; Wu, W.-W.; Bai, J.; Chen, L. J.; Tu, K. N.; Huang, Y. *Nano Lett.* **2008**, *8*, 913.
(27) Hsin, C.-L.; Lee, W.-F.; Huang, C.-T.; Huang, C.-W.; Wu, W.-W.; Chen, L.-J. *Nano Lett.* **2011**, *11*, 4348.
(28) Hsin, C.-L.; Wu, W.-W.; Chu, L.-W.; Hsu, H.-C.; Chen, L.-J. *CrystEngComm* **2011**, *13*, 3967.
(29) Strukov, D. B.; Snider, G. S.; Stewart, D. R.; Williams, R. S. *Nature* **2008**, *453*, 80.
(30) Chae, S. C.; Lee, J. S.; Kim, S.; Lee, S. B.; Chang, S. H.; Liu, C.; Kahng, B.; Shin, H.; Kim, D.-W.; Jung, C. U.; Seo, S.; Lee, M.-J.; Noh, T. W. *Adv. Mater.* **2008**, *20*, 1154.
(31) Waser, R.; Dittmann, R.; Staikov, G.; Szot, K. *Adv. Mater.* **2009**, *21*, 2632.
(32) Yu, S.; Wong, H.-S. P. *IEEE Electron Device Lett.* **2010**, *31*, 1455.
(33) Gao, B.; Kang, J. F.; Chen, Y. S.; Zhang, F. F.; Chen, B.; Huang, P.; Liu, L. F.; Liu, X. Y.; Wang, Y. Y.; Tran, X. A.; Wang, Z. R.; Yu, H. Y.; Chin, A. *Int. Electron Device Meeting* **2011**, *17*, 4u.